

2 **Improved Neutrino-Induced-Muon Momentum**
3 **Determination by Multiple Coulomb Scattering in the**
4 **MicroBooNE LArTPC from Tuning the Highland**
5 **Formula**

6 **The MicroBooNE Collaboration**

7 **ABSTRACT:** Liquid argon time projection chambers (LArTPCs) are an important detector technology for neutrino physics. This technology provides precise three-dimensional reconstruction of charged particle tracks that traverse the detector medium. We discuss a technique for measuring a charged particle's momentum by means of multiple Coulomb scattering (MCS) in the MicroBooNE LArTPC, which does not require the full particle ionization track to be contained inside of the detector volume as other track momentum reconstruction methods do (range-based momentum reconstruction and calorimetric momentum reconstruction). We motivate use of this technique, prescribe a tuning of the underlying theory formula, quantify its performance on fully contained beam-neutrino-induced muon tracks both in simulation and in data, and quantify its performance on exiting muon tracks in simulation. We find agreement between data and simulation for contained tracks, with a small bias in the momentum reconstruction and with resolutions that vary as a function of track length, decreasing from about 10% for the shortest (one meter long) tracks to 5% for longer (several meter) tracks. For exiting muons with at least one meter of track contained, we find a similarly small bias, and a resolution which is better than 15% for muons with momentum below 2 GeV though worse at higher momenta due to detector resolution effects.

22	Contents	
23	1 Introduction and Motivation	1
24	2 Multiple Coulomb Scattering (MCS)	3
25	2.1 Tuning the Highland Formula for Argon	4
26	3 MCS Implementation Using the Maximum Likelihood Method	6
27	3.1 Track Segmentation and Scattering Angle Computation	7
28	3.2 Maximum Likelihood Theory	7
29	3.3 Maximum Likelihood Implementation	8
30	4 Range-based Energy Validation from Simulation	8
31	5 MCS Performance on Beam Neutrino-Induced Muons in MicroBooNE Data	8
32	5.1 Input Sample	8
33	5.2 Event Selection	9
34	5.3 Highland Validation	10
35	5.4 MCS Momentum Validation	10
36	5.5 Impact of Highland Formula Tuning	12
37	6 MCS Performance on Existing Muons in MicroBooNE Simulation	13
38	7 Conclusions	14

39 **1 Introduction and Motivation**

40 MicroBooNE (Micro Booster Neutrino Experiment) is an R&D experiment that uses a large Liquid
41 Argon Time Projection Chamber (LArTPC) to investigate the excess of low energy events observed
42 by the MiniBooNE experiment [1] and to study neutrino-argon cross-sections. MicroBooNE is part
43 of the Short-Baseline Neutrino (SBN) physics program at the Fermi National Accelerator Labora-
44 tory (Fermilab) along with two other LArTPCs: the Short Baseline Near Detector (SBND) and
45 the Imaging Cosmic And Rare Underground Signal (ICARUS) detector. MicroBooNE also per-
46 forms important research and development in terms of detector technology and event reconstruc-
47 tion techniques for future LArTPC experiments including DUNE (Deep Underground Neutrino
48 Experiment).

49
50 The MicroBooNE detector[2] consists of a rectangular time projection chamber (TPC) with
51 dimensions 2.6 m width \times 2.3 m height \times 10.4 m length located 470 m away from the Booster
52 Neutrino Beam (BNB) target. LArTPCs allow for precise three-dimensional reconstruction of par-
53 ticle interactions. The x - direction of the TPC corresponds to the drift coordinate, the y - direction

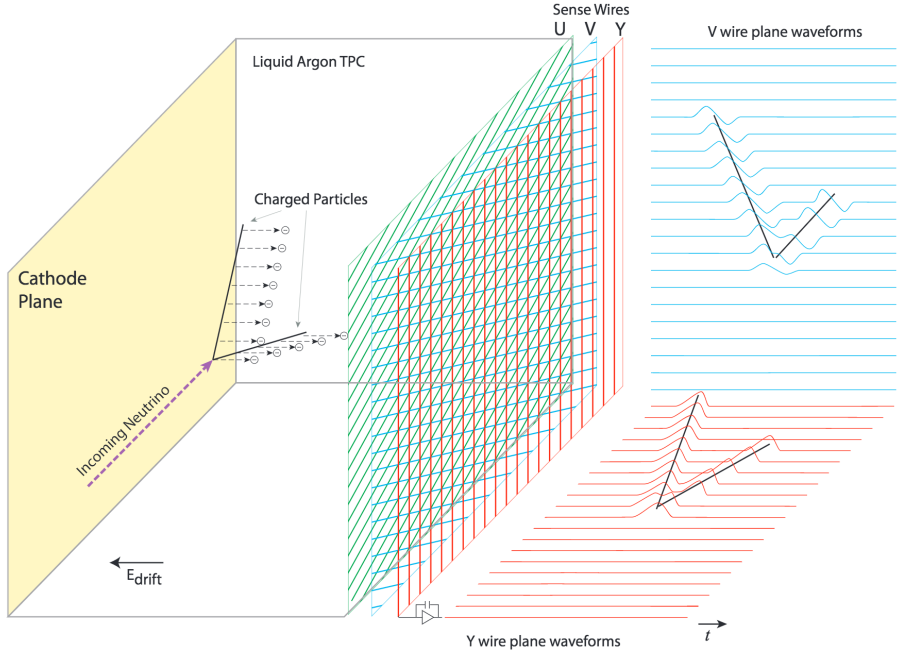


Figure 1. A diagram of the time projection chamber of the MicroBooNE detector [3]. PMTs (not shown) are located behind the wire planes.

is the vertical direction, and the $z-$ direction is the direction along the beam. The mass of active liquid argon in the MicroBooNE TPC is 89 tons, with the total cryostat containing 170 tons of liquid argon.

57

A set of 32 photomultiplier tubes (PMTs) and three planes of wires with 3 mm spacing at angles of 0, and ± 60 degrees with respect to the vertical are located in the TPC for event reconstruction (Figure 1). The cathode plane operating voltage is -70 kV. In a neutrino interaction, a neutrino from the beam interacts with an argon nucleus and the charged outgoing secondary particles traverse the medium, losing energy and leaving an ionization trail. The resulting ionization electrons drift to the anode side of the TPC, containing the wire planes. The passage of these electrons past the first two wire planes induces a signal in them, and their collection on the third plane also generates a signal. These signals are used to create three distinct two-dimensional views (in terms of wire and time) of the event. Combining these wire signals with timing information from the PMTs allows for full three-dimensional reconstruction of the event. The fiducial volume used in this analysis is defined as the full TPC volume reduced by 20 cm from both the cathode plane and the anode wire planes, by 26.5 cm from both the top and bottom walls of the TPC, by 20 cm from the beam-entering wall of the TPC, and by 36.8 cm from the beam-exiting wall of the TPC. This fiducial volume, corresponding to a mass of 55 tons, was chosen to reduce the impact of electric field nonuniformities near the edges of the TPC.

73
 74 The Booster Neutrino Beam (BNB) is predominantly composed of muon neutrinos (ν_μ) with
 75 a peak neutrino energy of about 0.7 GeV, some of which undergo charge-current (ν_μ CC) interac-
 76 tions in the TPC and produce muons. For muon tracks that are completely contained in the TPC,
 77 it is straightforward to calculate their momentum with a measurement of the length of the parti-
 78 cle's track, or with calorimetric measurements which come from wire signal size measurements.
 79 However, around half of the muons from BNB ν_μ CC interactions in MicroBooNE are not fully
 80 contained in the TPC, and therefore using length-based calculations for these uncontained tracks is
 81 not a possibility. The only way to compute the energy of a non-contained three-dimensional track
 82 is by means of multiple Coulomb scattering (MCS).
 83

84 In this paper we describe the theory behind multiple Coulomb scattering and a maximum
 85 likelihood based algorithm that is used to determine the momentum of particles in a LArTPC.
 86 That this technique works and is valid for a sample of fully contained muons from BNB ν_μ CC
 87 interactions is demonstrated, with bias and resolutions quantified. Additionally, quantification of
 88 performance on exiting tracks is presented.

89 2 Multiple Coulomb Scattering (MCS)

90 Multiple Coulomb scattering (MCS) occurs when a charged particle enters a medium and under-
 91 goes electromagnetic scattering with atomic nuclei. This scattering perturbs the original trajectory
 92 of the particle within the material (Figure 2). For a given energy, the angular deflection scatters of
 93 a particle in either the x' direction or y' direction (as indicated in the aforementioned figure) form
 94 a Gaussian distribution centered at zero with an RMS width, σ_o^{HL} given by the Highland formula
 95 [4]:
 96

$$\sigma_o^{HL} = \frac{13.6 \text{ MeV}}{p\beta c} z \sqrt{\frac{\ell}{X_0}} \left[1 + 0.0038 \times \ln\left(\frac{\ell}{X_0}\right) \right] \quad (2.1)$$

96 where β is the ratio of the particle's velocity to the speed of light assuming the particle is a muon,
 97 ℓ is the distance traveled inside the material, z is the magnitude of the charge of the particle, and
 98 X_0 is the radiation length of the target material (taken to be a constant 14 cm in liquid argon). In
 99 practice, a modified version of the Highland formula is used

$$\sigma_o = \sqrt{(\sigma_o^{HL})^2 + (\sigma_o^{res})^2} = \sqrt{\left(\frac{13.6 \text{ MeV}}{p\beta c} z \sqrt{\frac{\ell}{X_0}} \left[1 + 0.0038 \ln\left(\frac{\ell}{X_0}\right) \right] \right)^2 + (\sigma_o^{res})^2} \quad (2.2)$$

100 where the formula is “modified” from the original Highland formula (Equation 2.1) in that it in-
 101 cludes a detector-inherent angular resolution term, σ_o^{res} . For this analysis, this term is given a
 102 fixed value of 3 mrad which has been determined to be an acceptable value based on simulation
 103 studies of higher momenta muons. At 4.5 GeV/c muon momentum, Equation 2.1 predicts an RMS
 104 angular scatter of 3 mrad, comparable to the detector resolution, when $\ell \approx X_0$ as is the case in this
 105 study; the fully contained muons addressed in this analysis have momenta below 1.5 GeV making

106 detector resolution negligible.

107

108 With the Highland formula, the momentum of a track-like particle can be determined using
109 only the 3D reconstructed track it produces in the detector, without any calorimetric or track range
110 information. Within neutrino physics, past emulsion detectors like the DONUT [5] and OPERA [6]
111 experiments have used MCS to determine particle momenta. Additionally, the MACRO [7] experi-
112 ment at Gran Sasso Laboratory utilized this technique as well. While the original method for using
113 MCS to determine particle momentum in a LArTPC used a Kalman Filter and was described by
114 the ICARUS collaboration [8] (more recently the ICARUS collaboration describes another method
115 [9]), the maximum-likelihood based method discussed in this paper for use in the MicroBooNE
116 detector is described in detail in Section 3.

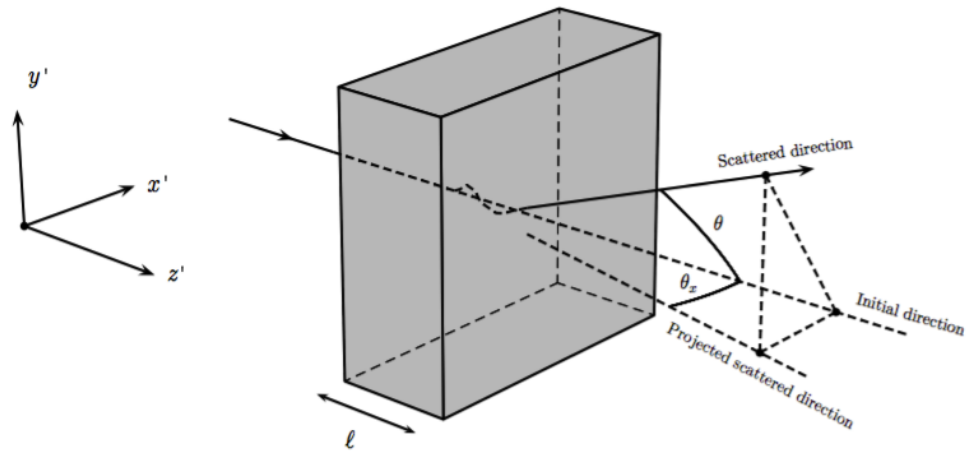


Figure 2. The particle’s trajectory is deflected as it traverses through the material.

117 2.1 Tuning the Highland Formula for Argon

118 The Highland formula as written in Equation 2.1 originated from a 1991 publication by G. R.
119 Lynch and O. I. Dahl [10]. The constants in the equation (13.6 and 0.0038) were determined using
120 a global fit over MCS simulated data using a modified GEANT simulation package of 14 differ-
121 ent elements and 7 thickness ranges. All of the simulated particles were relativistic, with $\beta = 1$.
122 The materials in which they studied scattering ranged from hydrogen (with $Z=1$) to uranium (with
123 $Z=92$). Given that the constants in the formula were determined from a single fit to a wide range of
124 Z with a wide range of material thicknesses, there is reason to believe that these constants should
125 differ for scattering specifically in liquid argon with $l \approx X_0$. There is also reason to believe that
126 these constants might be momentum-dependent for particles with $\beta < 1$, which is the case for
127 some of the contained muons in this analysis.

128

129 In order to re-tune these constants to liquid argon, a large sample of muons were simulated
130 with GEANT4 [11] in the MicroBooNE TPC and their true angular scatters were used in a fit,

131 with $l = X_0$. The reason for using $l = X_0$ is that the Highland equation simplifies to remove its
 132 dependence on the 0.0038 constant:

$$\sigma_o = \frac{13.6 \text{ MeV}}{p\beta c} \quad (2.3)$$

133 The 13.6 constant in Equation 2.3 was fit for as a function of true muon momentum at each
 134 scatter, in order to explore the β dependence of this constant. The fitted constant value as a function
 135 of true momentum is shown in Figure 3.

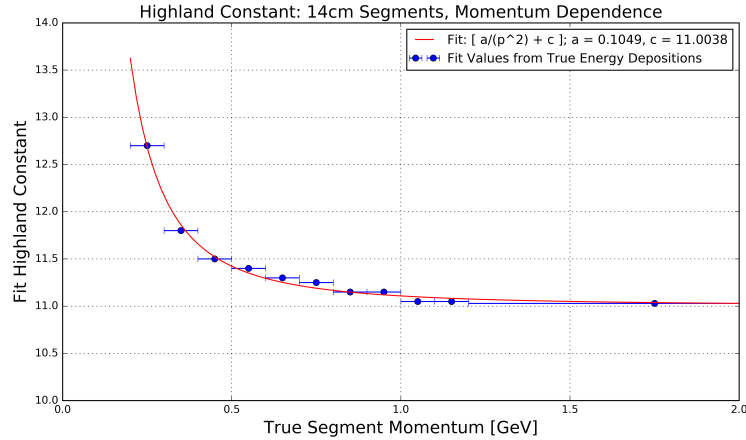


Figure 3. Fitted Highland constant as a function of true segment momentum for $l = X_0$ simulated muons in the MicroBooNE LArTPC. Blue x- error bars indicate the true momentum bin width with data points drawn at the center of each bin. Shown in red is a fit to these data points with functional form $\frac{a}{p^2} + c$, with best fit values for constants a and c shown in the legend.

136 It can be seen that the fitted value is always less than the nominal 13.6 for momentum greater
 137 than 0.25 GeV/c and asymptotically approaches a constant at higher momentum (where $\beta = 1$)
 138 of about 11.0. The value increases in the momentum region where $\beta < 1$. Shown in red is a fit
 139 to these data points with functional form $\frac{a}{p^2} + c$, with best fit values for floating constants a and
 140 c being 0.1049 and 11.0038 respectively. This functional form was chosen because it fit the data
 141 well, and asymptotically approaches a constant value when β approaches 1. This function, used as
 142 a replacement for the 13.6 constant in the Highland formula, will henceforth be referred to as $\kappa(p)$:

$$\kappa(p) = \frac{0.1049}{p^2} + 11.0038 \quad (2.4)$$

143
 144 To visualize the Highland formula for $l = X_0$ both before and after the $\kappa(p)$ replacement,
 145 see Figure 4. It is recommended that future LArTPC experiments use this parameterization of the
 146 Highland formula, or at the very least conduct their own studies to tune the Highland formula for
 147 scattering specifically in argon.
 148

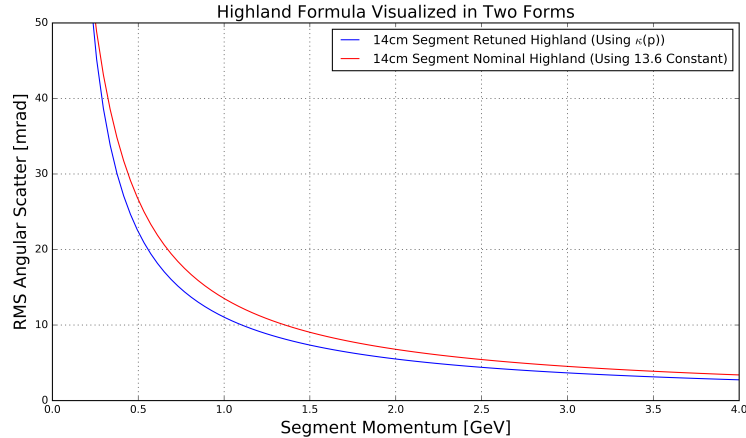


Figure 4. The Highland scattering RMS σ_o for 14 cm segment lengths and 0 detector-inherent angular resolution as a function of true momentum before and after tuning. In red is shown Equation 2.3 (the nominal Highland formula using the 13.6 constant) and in blue is the retuned Highland formula (replacing 13.6 with $\kappa(p)$).

149 The form of the Highland equation used in this analysis is therefore:

$$\sigma_o^{RMS} = \sqrt{(\sigma_o)^2 + (\sigma_o^{res})^2} = \sqrt{\left(\frac{\kappa(p)}{p\beta c} z \sqrt{\frac{\ell}{X_0}} \left[1 + 0.0038 \ln\left(\frac{\ell}{X_0}\right)\right]\right)^2 + (\sigma_o^{res})^2} \quad (2.5)$$

150 Note that with segmentation length $\ell = X_0 = 14\text{cm}$ the formula simplifies to remove the dependence
151 on the 0.0038 constant.

152 3 MCS Implementation Using the Maximum Likelihood Method

153 This section describes exactly how the phenomenon of multiple Coulomb scattering is leveraged
154 to determine the momentum of a muon track reconstructed in a LArTPC. In general, the approach
155 is as follows:

- 156 1. The three-dimensional track is divided into segments of configurable length.
 - 157 2. The scattering angles between consecutive segments are measured.
 - 158 3. Those angles combined with the modified, tuned Highland formula (Equation 2.5) are used
159 to build a likelihood that the particle has a specific momentum, taking into account energy
160 loss in upstream segments of the track.
 - 161 4. The momentum corresponding to the maximum of the likelihood is chosen to be the MCS
162 computed momentum.
- 163 Each of these steps is discussed in detail in the following subsections.

164

165 **3.1 Track Segmentation and Scattering Angle Computation**

166 Track segmentation refers to the subdivision of three-dimensional reconstructed trajectory points
167 of a reconstructed track into portions of definite length. In this analysis, the tracks are automatically
168 reconstructed by the “pandoraNuPMA” projection matching algorithm which constructs the
169 three-dimensional trajectory points by combining two-dimensional hits reconstructed from signals
170 on the different wire planes along with timing information from the photomultiplier tubes to re-
171 construct the third dimension [12]. The segmentation routine begins at the start of the track, and
172 iterates through the trajectory points in order, defining segment start and stop points based on the
173 straight-line distance between them. There is no overlap between segments. Given the subset
174 of the three-dimensional trajectory points that corresponds to one segment of the track, a three-
175 dimensional linear fit is applied to the data points, weighting all trajectory points equally in the
176 fit. In this analysis, a segment length of 14 cm is used, which is a tunable parameter that has been
177 optimized based on simulation studies.

178
179 With the segments defined, the scattering angles between the linear fits from adjacent segments
180 are computed. A coordinate transformation is performed such that the z' direction is oriented along
181 the direction of the linear fit to the first of the segment pair. The x' and y' coordinates are then
182 defined such that all of x' , y' , and z' are mutually orthogonal, as shown in Figure 2. The scattering
183 angles both with respect to the x' direction and the y' direction are then computed to be used by
184 the MCS algorithm. Note that only the scattering angle with respect to the x' direction is drawn in
185 Figure 2.

186 **3.2 Maximum Likelihood Theory**

187 The normal probability distribution for a scattering angle in either the x' or y' direction, $\Delta\theta$ with
188 an expected gaussian error σ_o and mean of zero is given by:

$$f_X(\Delta\theta) = (2\pi\sigma_o^2)^{-\frac{1}{2}} \exp\left(-\frac{1}{2}\left(\frac{\Delta\theta}{\sigma_o}\right)^2\right) \quad (3.1)$$

189 Here, σ_o is the RMS angular deflection computed by the modified, tuned Highland formula
190 (Equation 2.5), which is a function of both the momentum and the length of that segment. Since
191 energy is lost between segments along the track, σ_o increases for each angular measurement along
192 the track so we replace σ_o with $\sigma_{o,j}$, where j is an index representative of the segment.

193
194 To get the likelihood, one takes the product of $f_X(\Delta\theta_j)$ over all n of the $\Delta\theta_j$ segment-to-
195 segment scatters along the track. With some manipulation, this product becomes

$$L(\sigma_{o,1}, \dots, \sigma_{o,n}; \Delta\theta_1, \dots, \Delta\theta_n) = (2\pi)^{-\frac{n}{2}} \times \prod_{j=1}^n (\sigma_{o,j})^{-1} \times \exp\left(-\frac{1}{2} \sum_{j=1}^n \left(\frac{\Delta\theta_j}{\sigma_{o,j}}\right)^2\right) \quad (3.2)$$

196 In practice, rather than maximizing the likelihood it is more computationally convenient to
197 instead minimize the negative log likelihood. Inverting the sign and taking the natural logarithm of
198 the likelihood L gives an expression that is related to a χ^2

$$-\ln(L) = -\ln(L) = \frac{n}{2} \ln(2\pi) + \sum_{j=1}^n \ln(\sigma_{o,j}) + \frac{1}{2} \sum_{j=1}^n \left(\frac{\Delta\theta_j}{\sigma_{o,j}}\right)^2 \quad (3.3)$$

199 **3.3 Maximum Likelihood Implementation**

200 Given a set of angular deflections in the x' and y' directions for each segment as described in
201 Section 3.1 a raster scan over the postulated initial energy, E_t , in steps of 1 MeV up to 7.5 GeV is
202 computed and the step with the smallest negative log likelihood (Equation 3.3) is chosen as the final
203 MCS energy. Note that Equation 3.3 includes a $\sigma_{o,j}$ term which changes for consecutive segments
204 because their energy is decreasing. The energy of the j th segment is related to E_t by

$$E_j = E_t - E_j^{\text{upstream}} \quad (3.4)$$

205 where E_j^{upstream} is the energy loss upstream of this segment, computed by integrating the muon
206 stopping power curve given by the Particle Data Group (PDG) [14] along the length of track up-
207 stream of this segment. Note that Equation 3.4 introduces a minimum allowable track energy
208 determined by the length of the track, as E_j must remain positive. This value of segment energy is
209 converted to a momentum, p , with the usual energy-momentum relation assuming the muon mass,
210 and is then used to predict the RMS angular scatter for that segment (σ_o) by way of Equation 2.5.

211 **4 Range-based Energy Validation from Simulation**

212 In order to quantify the performance of the MCS energy estimation method on fully contained
213 muons in data, an additional handle on energy is needed. Here, range-based energy, E_{range} is used
214 since when dealing with data the true energy, E_{true} will not be known. The stopping power of
215 muons in liquid argon is well described by the continuous-slowing-down-approximation (CSDA)
216 by the particle data group (PDG) with agreement to data at the sub-percent level [13] [15] [16].
217 By using a linear interpolation between points in the cited PDG stopping power table, the length
218 of a track can be used to reconstruct the muon's total energy with good accuracy. A simulated
219 sample of fully contained BNB neutrino-induced muons longer than one meter is used to quantify
220 the bias and resolution for the range-based energy estimation technique. The range is defined as
221 the straight-line distance between the true starting point and true stopping point of a muon. The
222 bias and resolution are computed in bins of true total energy of the muons by fitting a gaussian to
223 a distribution of the fractional energy difference ($\frac{E_{\text{Range}} - E_{\text{True}}}{E_{\text{True}}}$) in each bin. The mean of each
224 gaussian indicates the bias for that true energy bin, and the width indicates the resolution. Figure
225 5 shows the bias and resolution for the range-based energy reconstruction method. It can be seen
226 that the bias is negligible and the resolution for this method of energy reconstruction is on the
227 order of 2-4%. Based on this figure, it is clear that range-based energy (and therefore range-based
228 momentum) is a good handle on the true energy (momentum) of a reconstructed muon track in
229 data, assuming that the track is well reconstructed in terms of length.

230 **5 MCS Performance on Beam Neutrino-Induced Muons in MicroBooNE Data**

231 **5.1 Input Sample**

232 The input sample to this portion of the analysis is $\sim 5 \times 10^{19}$ protons-on-target worth of trig-
233 gered BNB neutrino interactions in MicroBooNE data, which is a small subset (less than 10%)
234 of the nominal amount of beam scheduled to be delivered to the detector. These events are run

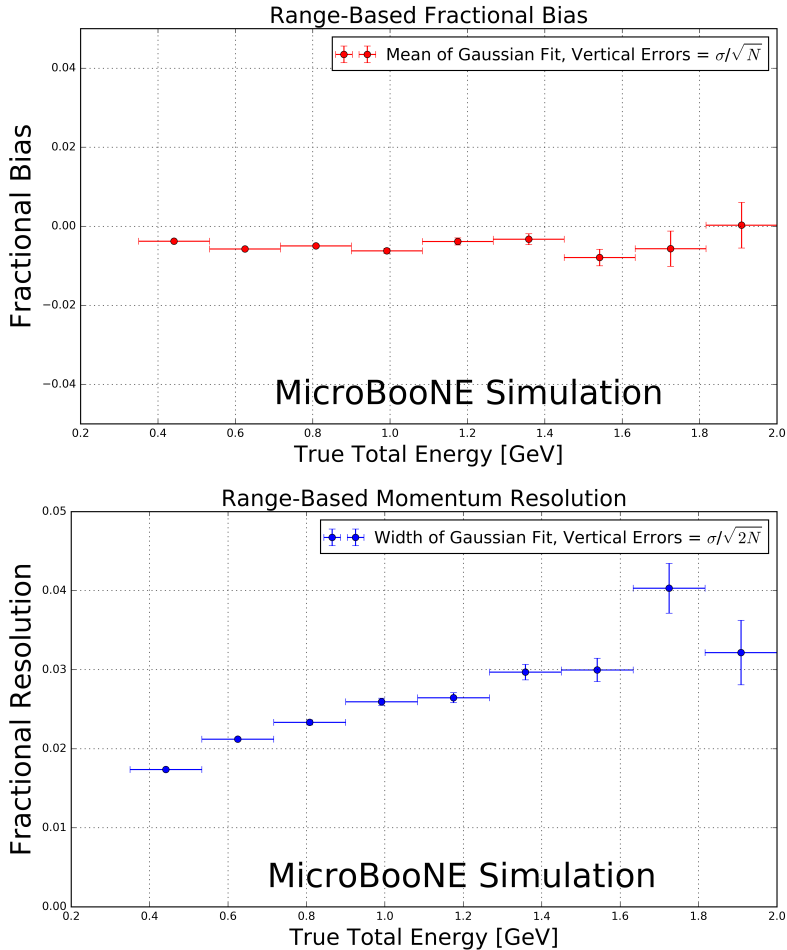


Figure 5. Range-based energy fractional bias (top) and resolution (bottom) from a sample of simulated fully contained BNB neutrino-induced muons using true starting and stopping positions of the track. The bias is less than 1% and the resolution is below $\approx 4\%$.

through a fully automated reconstruction chain which produces reconstructed objects including three-dimensional neutrino interaction points (vertices), three-dimensional tracks for each outgoing secondary particle from the interaction, and PMT-reconstructed optical flashes from the interaction scintillation light. The fiducial volume used in this analysis is defined in Section 1.

5.2 Event Selection

The following selection cuts are placed on the aforementioned reconstructed objects to select ν_μ charged-current interactions in which a candidate muon track exiting the interaction vertex is fully contained within the fiducial volume:

1. The event must have at least one bright optical flash in coincidence with the expected BNB neutrino arrival time.
2. Two or more reconstructed tracks must originate from the same reconstructed vertex within the fiducial volume.

- 247 3. The span in z – of the candidate muon track must be within 70 cm of the z – position of the
 248 optical flash as determined by the pulse height and timing of signals in the 32 PMTs.
- 249 4. For events with exactly two tracks originating from the vertex, additional calorimetric-based
 250 cuts are applied to mitigate backgrounds from cosmics in time with the passage of the beam
 251 which produce a Michel electron reconstructed as a track.
- 252 5. The longest track originating from the vertex is assumed to be a muon, and it must be fully
 253 contained within the fiducial volume.
- 254 6. The longest track must be at least one meter long, in order to have enough sampling points
 255 in the MCS likelihood to obtain a reasonable estimate of its momentum.

256 In this sample of MicroBooNE data, 598 events (tracks) remain after all event selection cuts.
 257 The relatively low statistics in this sample is due to the limited input sample, described in Sec-
 258 tion 5.1. Each of these events (tracks) were scanned by hand with a 2D interactive event display
 259 showing the raw wire signals of the interaction from each wire plane, with the 2D projection of the
 260 reconstructed muon track and vertex overlaid. The scanning was done to ensure the track was well
 261 reconstructed with start point close to the reconstructed vertex and end point close to the end of the
 262 visible wire-signal track in all three planes. Additionally the scanning was to remove obvious mis-
 263 identification (MID) topologies such as cosmic rays inducing Michel electrons at the reconstructed
 264 neutrino vertex which were not successfully removed by the automated event selection cuts. After
 265 rejecting events (tracks) based on hand scanning, 396 tracks remain for analysis.

266 5.3 Highland Validation

267 The Highland formula indicates that histograms of the track segment-by-segment angular devia-
 268 tions in both the x' and y' directions divided by the width predicted from the Highland equation
 269 σ_o^{HL} (Equation 2.5) should be gaussian with a width of unity. In order to calculate the momentum
 270 p in the Highland equation, p for each segment is computed with Equation 3.4 where E_t comes
 271 from the converged MCS computed momentum of the track. For each consecutive pair of segments
 272 in this sample of 396 tracks, the angular scatter in milliradians divided by the Highland expected
 273 RMS in milliradians is an entry in the area-normalized histogram shown in Figure 6. From this
 274 figure we can see that the distribution has an RMS of unity, thus validating the MCS technique
 275 used in this analysis.

276 5.4 MCS Momentum Validation

277 The MCS momentum versus range-based momentum for this sample of 396 tracks can be seen
 278 in Figure 7. The fractional bias and resolution as a function of range-based momentum for this
 279 sample is shown in Figure 8. In order to compute this bias and resolution, distributions of frac-
 280 tional inverse momentum difference ($\frac{p_{MCS}^{-1} - p_{Range}^{-1}}{p_{Range}^{-1}}$) in bins of range-based momentum p_{Range}
 281 are fit to gaussians and the mean of the fit determines the bias while the width of the fit determines
 282 the resolution for that bin. Inverse momentum is used here because the binned distributions are
 283 more gaussian (since the Highland formula measures inverse momentum in terms of track angles
 284 that have reasonably Gaussian errors). Note that simply using the mean and RMS of the binned

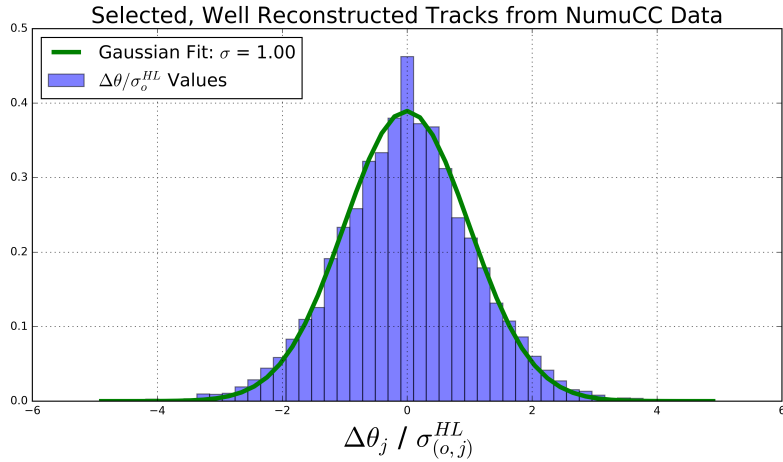


Figure 6. Segment-to-segment measured angular scatters in both the x' and y' directions divided by the Highland formula (Equation 2.1) predicted width σ_o^{HL} for the automatically selected beam neutrino-induced fully contained muon sample in MicroBooNE data after hand scanning to remove poorly reconstructed tracks and obvious mis-identification (MID) topologies. That the fitted Gaussian distribution has a width of unity indicates that the basis of the MCS technique is validated.

285 distributions yields similar results. Also shown in this figure are the bias and resolutions for an anal-
 286 ogous simulated sample consisting of full BNB simulation with CORSIKA-generated [17] cosmic
 287 overlays passed through an identical reconstruction and event selection chain. Rather than hand
 288 scanning this sample, true simulation information was used by requiring the longest reconstructed
 289 track matched well in terms of true starting and stopping point of the ν_μ CC muon. This removes
 290 any mis identifications or interference from the simulated cosmics.

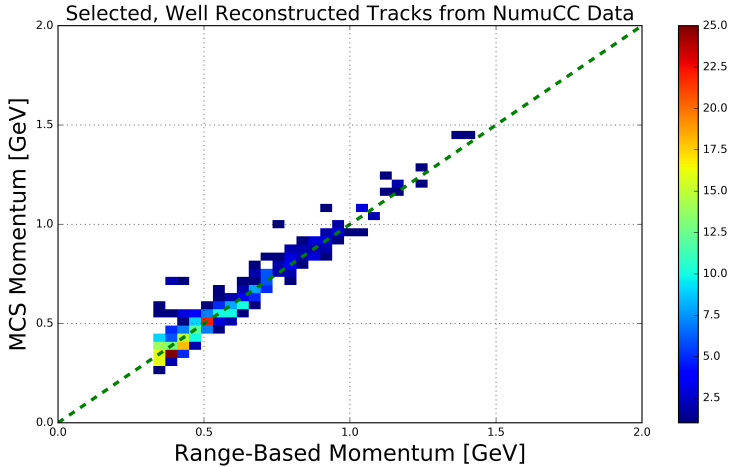


Figure 7. MCS computed momentum versus range momentum for the automatically selected beam neutrino-induced fully contained muon sample in MicroBooNE data after hand scanning to remove poorly reconstructed tracks and obvious mis-identification (MID) topologies. The color (z) scale indicates number of tracks.

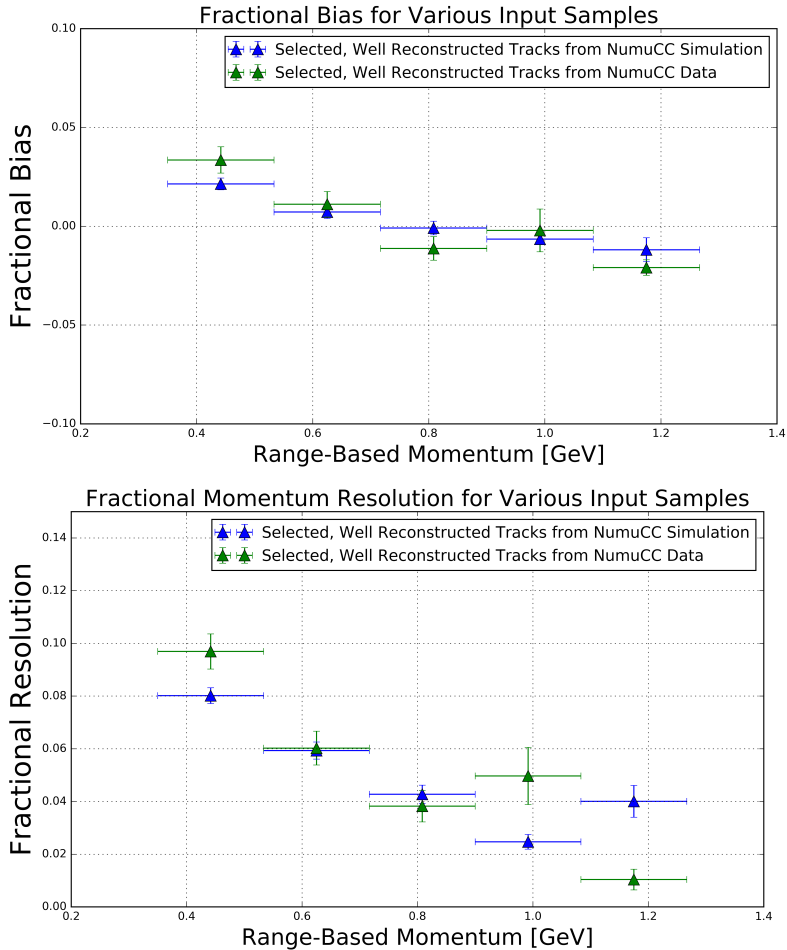


Figure 8. Inverse momentum difference (as defined in the text) fractional bias (top) and resolution (bottom) for automatically selected contained ν_μ CC-induced muons from full simulated BNB events with cosmic overlay where the track matches with the true muon track (blue), and automatically selected (see text) contained ν_μ CC-induced muons from MicroBooNE data (green).

291 Figure 8 indicates a bias in the MCS momentum calculation on the order of a few percent, with
 292 a resolution that decreases from about 10% for contained reconstructed tracks in data and simula-
 293 tion with range momentum around 0.45 GeV (which corresponds to a length of about 1.5 meters)
 294 to below 5% for contained reconstructed tracks in data and simulation with range momentum about
 295 1.15 GeV (which corresponds to a length of about 4.6 meters). In general the bias and resolutions
 296 agree between data and simulation within uncertainty.
 297

298 5.5 Impact of Highland Formula Tuning

299 In order to examine the impact of the Highland formula tuning described in Section 2.1, the frac-
 300 tional bias and resolution on the simulated sample of contained muons described in Section 5.4
 301 both with the nominal Highland formula (Equation 2.2) and with the retuned Highland formula
 302 (Equation 2.5) are shown in Figure 9. Tuning the Highland formula improves the magnitude of

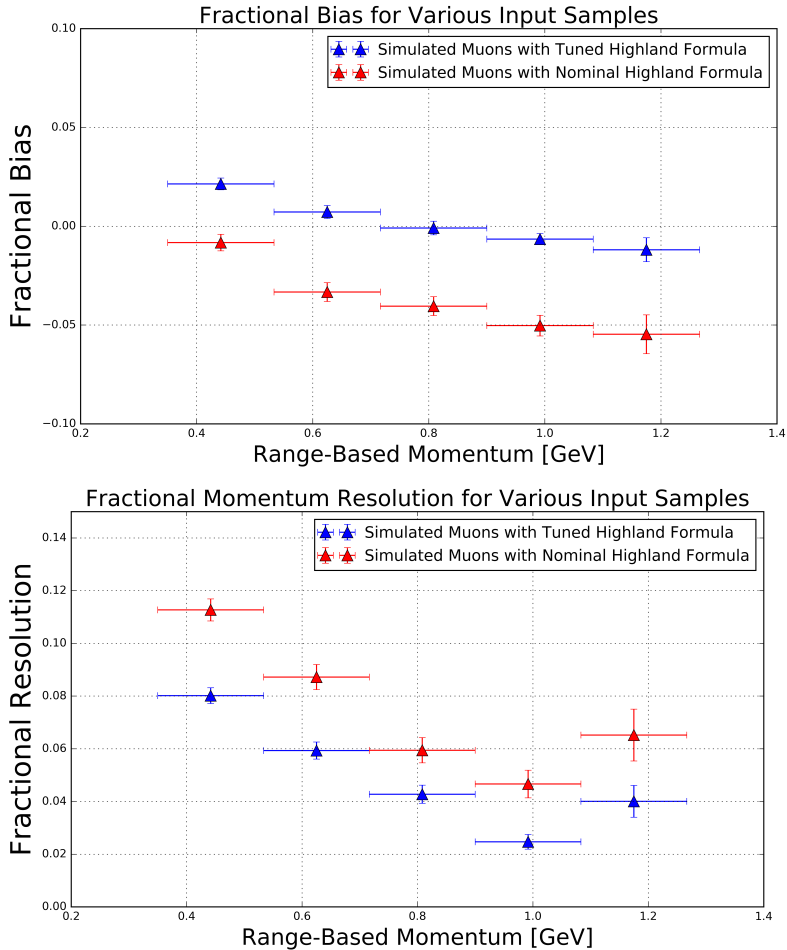


Figure 9. Inverse momentum difference (as defined in the text) fractional bias (top) and resolution (bottom) for automatically selected contained ν_μ CC-induced muons from full simulated BNB events with cosmic overlay where the track matches with the true muon track both using the nominal Highland formula (Equation 2.2) (red) and the retuned Highland formula (Equation 2.5) (blue).

303 the fractional bias to below 2%, and improves the fractional resolution by 2-3%, with the most
 304 improvement in the lowest momentum bins.

305 6 MCS Performance on Exiting Muons in MicroBooNE Simulation

306 This section quantifies the MCS algorithm performance on a sample of exiting muon tracks in
 307 simulated BNB ν_μ CC interactions within the MicroBooNE detector. The tracks are automatically
 308 reconstructed by the same ‘‘pandoraNuPMA’’ algorithm described in Section 3.1, and all tracks
 309 have at least one meter contained within the TPC. This simulation does not include space charge
 310 effects which are non-negligible near the TPC walls. The MCS momentum versus true momentum
 311 for this sample of 28,000 exiting muon tracks can be seen in Figure 10.
 312

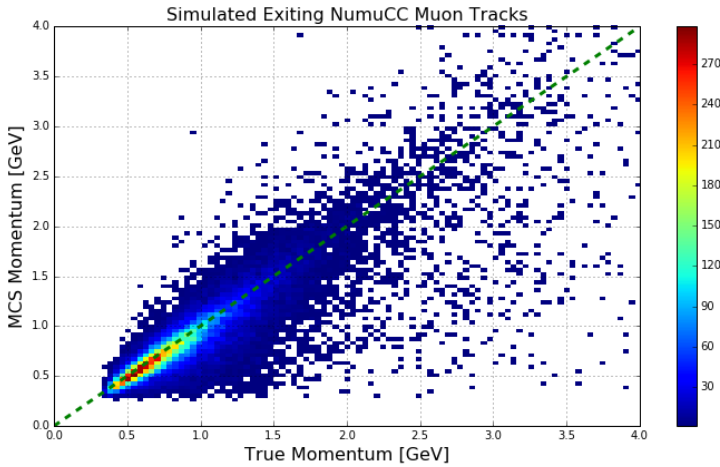


Figure 10. MCS computed momentum versus true momentum for the sample of simulated exiting BNB ν_μ CC muons in MicroBooNE with at least one meter of track contained within the TPC.

313 The distribution of $(\frac{p_{MCS}^{-1} - p_{true}^{-1}}{p_{true}^{-1}})$ is shown for four representative bins of true momentum in
 314 Figure 11, along with the Gaussian fit to each. Low momentum tails in which the MCS momentum
 315 is an underestimation of the true momentum can be seen outside of the central gaussian fit. These
 316 tails can be attributed to reconstruction effects.

317
 318 The algorithm fractional bias and resolution as a function of true momentum are shown in Fig-
 319 ure 12. It can be seen that the bias is below 4% for all momenta, and the resolution is roughly 14%
 320 in the relevant momentum region for BNB ν_μ CC muons (below 2 GeV). The resolution worsens
 321 for muon momenta above this region because the angular scatters begin to be comparable with the
 322 detector resolution term of 3 mrad. Note that the resolution improves for longer lengths of track
 323 contained, with 10% resolution for muons below 2 GeV with more than 3.5 meters contained. Res-
 324 olution improving with length of track is intuitive; the longer portion of track contained, the more
 325 angular scattering measurements can be made to improve the likelihood.
 326

327 7 Conclusions

328 We have described a multiple Coulomb scattering maximum likelihood method for estimating the
 329 momentum of a three dimensional reconstructed track in a LArTPC and have provided motivation
 330 for development of such a technique. This technique is a very valuable tool; it is the only way to
 331 estimate the momentum of an exiting muon and will be an important ingredient in future oscillation
 332 and cross-section measurements by MicroBooNE and within the LArTPC community as a whole.
 333 The performance of this method has been quantified both in simulation and in data on beam ν_μ CC-
 334 induced muons which are fully contained, with fractional bias less than 3% and with fractional
 335 resolution at or below 10%. The performance of this method has been quantified on exiting muon
 336 tracks in simulation, with resolution better than 15% for muons in the relevant BNB energy region
 337 below 2 GeV.

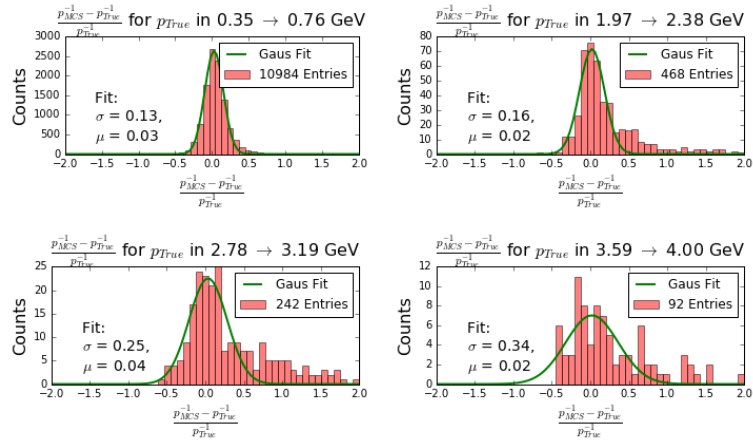


Figure 11. Fractional momentum difference for a few representative bins of true momentum.

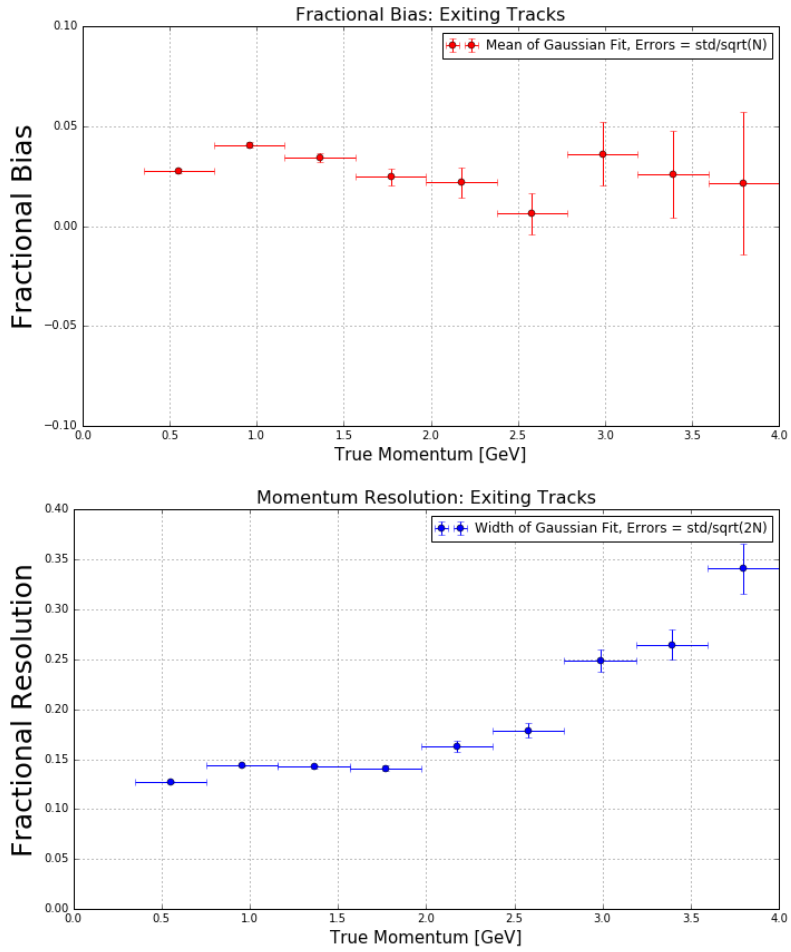


Figure 12. MCS momentum fractional bias (top) and resolution (bottom) as a function of true momentum from a sample of exiting reconstructed muon tracks.

338 **References**

- 339 [1] A. A. Aguilar-Arevalo *et al.* [MiniBooNE Collaboration], Improved Search for $\bar{\nu}_\mu \rightarrow \bar{\nu}_e$ Oscillations
340 in the MiniBooNE Experiment, Phys. Rev. Lett. **110**, 161801 (2013).
341 doi:10.1103/PhysRevLett.110.161801 [arXiv:1207.4809 [hep-ex], arXiv:1303.2588 [hep-ex]].
- 342 [2] R. Acciarri *et al.* [MicroBooNE Collaboration], “Design and Construction of the MicroBooNE
343 Detector,” arXiv:1612.05824 [physics.ins-det].
- 344 [3] S. Lockwitz, The MicroBooNE LArTPC,
345 <http://www-microboone.fnal.gov/talks/dpfMicroBooNELArTPC.pdf>.
- 346 [4] V. L. Highland, Some Practical Remarks on Multiple Scattering, Nucl. Instrum. Methods **129** (1975)
347 104-120.
- 348 [5] K. Kodama *et al.* [DONUT Collaboration], Phys. Lett. B **504**, 218 (2001)
349 doi:10.1016/S0370-2693(01)00307-0 [hep-ex/0012035].
- 350 [6] N. Agafonova *et al.* [OPERA Collaboration], New J. Phys. **14**, 013026 (2012)
351 doi:10.1088/1367-2630/14/1/013026 [arXiv:1106.6211 [physics.ins-det]].
- 352 [7] G. Giacomelli [MACRO Collaboration], Braz. J. Phys. **33**, 211 (2003)
353 doi:10.1590/S0103-97332003000200008 [hep-ex/0210006].
- 354 [8] A. Ankowski *et al.* [ICARUS Collaboration], “Measurement of through-going particle momentum by
355 means of multiple scattering with the ICARUS T600 TPC,” Eur. Phys. J. C **48**, 667 (2006)
356 doi:10.1140/epjc/s10052-006-0051-3 [hep-ex/0606006].
- 357 [9] M. Antonello *et al.*, “Muon momentum measurement in ICARUS-T600 LAr-TPC via multiple
358 scattering in few-GeV range,” arXiv:1612.07715 [physics.ins-det].
- 359 [10] G. R. Lynch and O. I. Dahl, Nucl. Instrum. Methods Section B (Beam Interactions with Materials
360 and Atoms) **B58**, **6** (1991).
- 361 [11] S. Agostinelli et al. Nucl. Instrum. Methods Phys. Res. **A506250-303** (2003)
- 362 [12] J. S. Marshall and M. A. Thomson, “The Pandora Software Development Kit for Pattern
363 Recognition,” Eur. Phys. J. C **75**, no. 9, 439 (2015) doi:10.1140/epjc/s10052-015-3659-3
364 [arXiv:1506.05348 [physics.data-an]].
- 365 [13] D. E. Groom, N. V. Mokhov and S. Striganov, “Muon Stopping Power and Range Tables: 10 MeV -
366 100 TeV” Table 5, <http://pdg.lbl.gov/2012/AtomicNuclearProperties/adndt.pdf>
- 367 [14] H. Bichsel, D. E. Groom, S.R. Klein, “Passage of Particles Through Matter” PDG Chapter 27, Figure
368 27.1 <http://pdg.lbl.gov/2005/reviews/passagerpp.pdf>
- 369 [15] Table 289: Muons in Liquid argon (Ar) http://pdg.lbl.gov/2012/AtomicNuclearProperties/MUON_ELOSS_TABLES/muonloss_289.pdf
- 370 [16] “Stopping Powers and Ranges for Protons and Alpha Particles,” ICRU Report No. 49 (1993); Tables
371 and graphs of these data are available at <http://physics.nist.gov/PhysRefData/>
- 372 [17] D. Heck, J. Knapp, J. N. Capdevielle, G. Schatz, T. Throw, *CORSIKA: A Monte Carlo Code to*
373 *Simulate Extensive Air Showers*, Forschungszentrum Karlsruhe Report FZKA 6019 (1998)